Simulation of Residual Water Radiolysis-Induced Material Degradation in a Dry Storage Canister

Sangjin Kim[a], Kwanil Chae[a], Samuel Park[a], Sungyeol Choi[a, b, c*]
[a] *Department of Nuclear Engineering, Seoul National University*
[b] *Nuclear Research Institute for Future Technology and Policy, Seoul National University*
[c] *Institute of Engineering Research, Seoul National University*
[*] *Corresponding author: choisys7@snu.ac.kr*

***Keywords: Corrosion kinetics, Electrochemical experiments, Residual water radiolysis, Temperature distribution modeling, Dry storage cask degradation progression.**

1. Introduction

South Korea's wet storage capacity for spent nuclear fuel (SNF) is expected to reach its limit by 2030, necessitating a transition to dry storage. While dry storage casks provide passive cooling and long-term containment, their structural integrity must be ensured over extended periods. A key concern is residual water remaining after vacuum drying, which, under radiation exposure, undergoes radiolysis, producing oxidizing species such as hydrogen peroxide (H_2O_2) [1]. These species may accelerate corrosion, potentially compromising material performance over time, and thus the integrity of the dry cask storage.

Despite the increasing global adoption of dry storage, the long-term impact of radiolysis-induced corrosion on AA6061 and SS17-4, key structural materials, remains unclear. To address this, this study investigates the degradation behavior of AA6061 and SS17-4 over a 50-year storage period using a 2D COMSOL Multiphysics model under H_2O_2-dominated conditions, where H_2O_2 serves as the primary oxidizing agent with its high standard reduction potential.

2. Methodology

This study consists of two main components: electrochemical experiments for Tafel parameter measurements and Thermal-Electrochemistry numerical modeling. To model the degradation effects in a dry storage cask, thermal modeling and electrochemical experiments were conducted beforehand to assess the temperature distribution inside the cask and to obtain corrosion kinetics data for AA6061 and SS17-4. The results from these analyses were then incorporated into the corrosion model for further evaluation.

2.1. Electrochemical experiments.

Electrochemical experiments were conducted under varying H_2O_2 concentrations and pH conditions to obtain Tafel polarization curves for corrosion kinetics, addressing the limitations of existing literature data. A three-electrode cell was configured, and a potentiostat was used to control potential and current, enabling the electrochemical monitoring of the corrosion reaction. A Saturated Calomel Electrode (SCE) was used as the reference electrode, chosen for its stability at room temperature and suitability for corrosion experiments, whereas the counter electrode was a platinum (Pt) electrode, selected for its high conductivity and inert properties, ensuring reliable test results. The maximum H_2O_2 concentration employed was 10^{-4} M, based on previous studies [2], while pH values (4–6) were selected to reflect wet storage pool conditions.

The experimental matrix used for corrosion behavior evaluation is presented in figure 1.

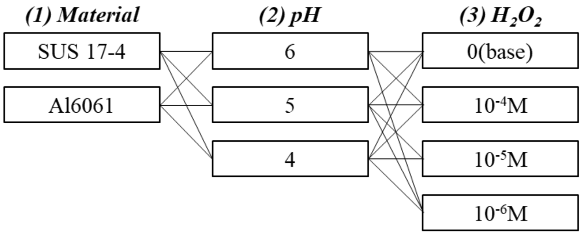

Fig. 1. Corrosion experiment matrix for evaluating corrosion behavior of dry storage container internal structural materials due to radiolysis products of residual moisture.

2.2. Computational analysis

2.2.1. Thermal model

A 3D thermal model was developed based on the geometry and design of KORAD-21, a Korean dry storage cask, incorporating conduction, radiation, and external natural convection via COMSOL Multiphysics. The decay heat from SNF with a burn-up of 45,000 MWd/tHM and 4.0 wt% enrichment was described using equation (1) for the first 30 years. Beyond this period, equation (2) was applied due to a shift in the dominant decay heat sources, as the influence of fission products diminishes and the contribution from actinides increases over time [3] It is assumed that the SNF was stored in a wet storage pool for 10 years before being transferred to the dry cask.

$$(1)\quad \mathbf{P(t)} = \mathbf{881.99} \times \boldsymbol{e}^{\frac{\mathbf{1}}{\mathbf{0.23990+141124\times(}\boldsymbol{t}\mathbf{+10)}}}\ [\boldsymbol{W/tHM}]$$

For 1 < t < 20 years

$$(2)\quad P(t) = 14545.68 \times (t+10)^{-0.75756}\ [W/tHM]$$
$$\text{For } 20 < t < 10^6 \text{ years}$$

The equation (3) was employed to simulate the heat transfer behavior of SNF inside the dry cask.

$$(3)\qquad \rho C_p\left(\frac{\partial T}{\partial t}\right) + \nabla\cdot(q+q_r) = Q$$

ρ is the density [kg/m³]
C_p: specific heat capacity at constant pressure
q: heat flux by conduction [W/m²]
q_r: heat flux by radiation [W/m²]
Q: additional heat sources [W/m3]

2.2.2. Corrosion model

The geometry is modeled in 2D, representing the electrolyte placed over the anode, as shown in figure 2. The model simulates the degradation of the anode over time due to corrosion effects. A triangular mesh was applied, with refined meshing at the surface of the internal structural materials to enhance accuracy. In total, 1,273 elements were used for the mesh.

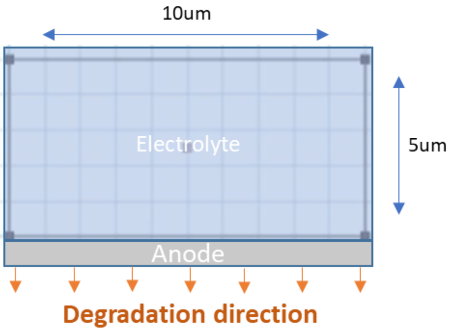

Fig. 2. Design and geometry of the uniform corrosion model.

The model incorporates the Nernst-Planck equation (4) to simulate mass transport, accounting for diffusion, migration, and convection within the electrolyte. Additionally, the Butler-Volmer equation (5) is used to describe the reaction kinetics at the electrode-electrolyte interface, governing the rate of electrochemical reactions.

$$(4)\qquad N_i = -D_i\nabla c_i - z_i u_{m,i} F c_i \nabla\phi_l + c_i u = J_i + c_i u$$

$-D_i\nabla c_i$: Diffusion term
$-z_i u_{m,i} F c_i \nabla\phi_l$: Migration term
$c_i u$: Convection term
$J_i + c_i u$: Combination of convective flux and additional flux

$$(5)\quad i_{loc} = i_0\left(\prod\left(\frac{c_i}{c_{i,ref}}\right)^{\gamma_{i,a}} \exp\left(\frac{\alpha_a F\eta}{RT}\right) - \prod\left(\frac{c_i}{c_{i,ref}}\right)^{\gamma_{i,c}} \exp\left(\frac{-\alpha_c F\eta}{RT}\right)\right)$$

α_a: anodic charge transfer coefficient
i_0: exchange current density [A/m2]
α_c: cathodic charge transfer coefficient
$\gamma_{i,a}$: anodic reaction order for species i
$\gamma_{i,c}$: cathodic reaction order for species i

The initial and boundary conditions, along with material properties, were obtained from the literature review and previous studies, including thermal model results and Tafel property measurements. The pH conditions range from 4 to 6, while the H_2O_2 concentration varies between 10^{-4} M and 10^{-6} M. The density, diffusion coefficients, and porosity values used in the corrosion modeling are summarized in the following table.

Table 1: Key parameters for corrosion modeling [4,5].

	Density [g/cm^3]	Porosity
AA6061	2.70	0.01
SS17-4	7.75	0.0386

	Diffusion coefficient [m^2/s]
Fe	7.19E-10
Al	5.59E-10
H_2O_2	2E-9
O_2	2.3E-9
H	0.37E-8
OH	5.3E-9

3. Result and discussion

3.1. Electrochemical experiments result

Table 2 summarizes the Tafel properties of SS17-4 and AA6061, presenting the electrochemical corrosion behavior as a function of pH and H_2O_2 concentration. It provides the measured values of corrosion potential (E_{corr}), corrosion current density (i_{corr}), and anodic Tafel slope (β_a) for each material.

Table 2: Tafel properties for SS17-4 (sus) and AA6061 (Al) under different H2O2 concentrations and pH levels.

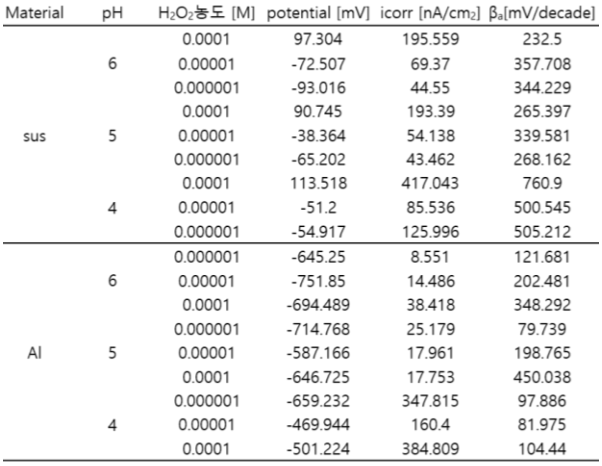

Material	pH	H_2O_2농도 [M]	potential [mV]	icorr [nA/cm$_2$]	β_a[mV/decade]
sus	6	0.0001	97.304	195.559	232.5
		0.00001	-72.507	69.37	357.708
		0.000001	-93.016	44.55	344.229
	5	0.0001	90.745	193.39	265.397
		0.00001	-38.364	54.138	339.581
		0.000001	-65.202	43.462	268.162
	4	0.0001	113.518	417.043	760.9
		0.00001	-51.2	85.536	500.545
		0.000001	-54.917	125.996	505.212
Al	6	0.000001	-645.25	8.551	121.681
		0.00001	-751.85	14.486	202.481
		0.0001	-694.489	38.418	348.292
	5	0.000001	-714.768	25.179	79.739
		0.00001	-587.166	17.961	198.765
		0.0001	-646.725	17.753	450.038
	4	0.000001	-659.232	347.815	97.886
		0.00001	-469.944	160.4	81.975
		0.0001	-501.224	384.809	104.44

3.2. Thermal model result

Figure 3 illustrates the temperature distribution over time inside the dry storage cask. The results indicate that the maximum temperature reaches approximately 274 °C over 100 years, while the overall temperature gradually decreases over time.

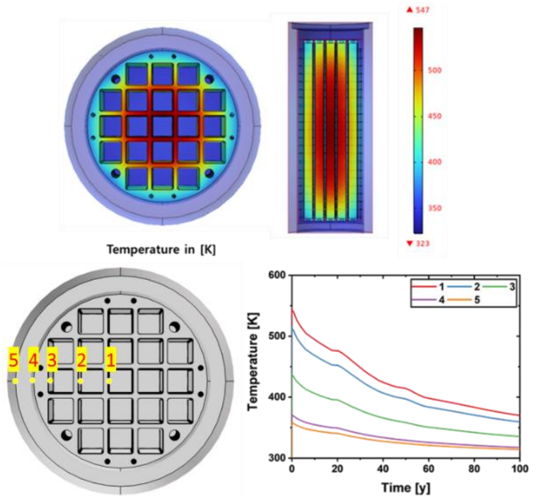

Fig. 3. Temperature distribution predicted by the thermal model.

3.3. Corrosion numerical model result

The simulation results indicate that both materials exhibit low corrosion rates, posing minimal risk to the long-term performance of the dry storage cask. However, as shown in figure 4, AA6061 demonstrated superior corrosion resistance compared to SS17-4. Over a 50-year period, under conditions of [H_2O_2] = 10^{-5} M and pH 5, the estimated degradation for AA6061, as predicted by the numerical model, is approximately 0.01475 mm, whereas SS17-4 exhibits a higher degradation of 0.0604 mm. This difference is attributed to the lower porosity of the oxide film on AA6061, which enhances its corrosion resistance. To ensure a conservative approach, the highest temperature evolution predicted by the thermal model was incorporated as a boundary condition to determine the maximum corrosion depth.

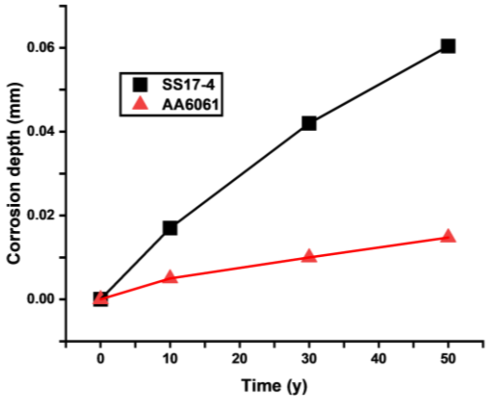

Fig. 4. Degradation progression of SS17-4 and AA6061 over 10 and 50 years in an environment with [H_2O_2] = 10^{-5} M and pH 5 as predicted by the corrosion model.

4. Conclusion

While pH and H_2O_2 concentration influence corrosion behavior, their overall impact remains limited. Both AA6061 and SS17-4 exhibit high corrosion resistance in radiolytic environments, with AA6061 demonstrating slightly superior resistance due to the lower oxide film porosity, which contributes to a more stable corrosion rate over time. This corrosion resistance ensures the long-term structural integrity of dry storage casks, even in the presence of residual moisture.

These findings provide valuable insights into radiolysis-induced corrosion mechanisms, reinforcing the suitability of AA6061 and SS17-4 for dry storage applications. However, further investigation is required to fully understand the influence of pH, H_2O_2 concentration, and temperature on the corrosion rate of each material. Ultimately, this study contributes to the development of more durable and resilient dry storage systems for SNF by improving the understanding of material degradation under radiolytic conditions.

5. Acknowledgments

This work was supported by the Korea Institute of Energy Technology Evaluation and Planning (KETEP) and the Ministry of Trade, Industry & Energy (MOTIE) of the Republic of Korea (No. 20224000000120).

REFERENCES

[1] Le Caër, Sophie. "Water radiolysis: influence of oxide surfaces on H2 production under ionizing radiation." Water 3.1(2011):235-253.
[2] Daub, K., et al. "Effects of γ-radiation versus H2O2 on carbon steel corrosion." Electrochimica Acta 55.8 (2010): 2767-2776.
[3] Choi, Heui Joo, Lee, J Y, and Kim, S S. Korean Reference HLW Disposal System. Korea, Republic of: N. p., 2008. Web.
[4] Tjell, Anders Ø., and Kristoffer Almdal. "Diffusion rate of hydrogen peroxide through water-swelled polyurethane membranes." Sensing and bio-sensing research 21 (2018): 35-39.
[5] Cheng, Tsung-Chieh, and Chu-Chiang Chou. "The Electrical and Mechanical Properties of Porous Anodic 6061-T6 Aluminum Alloy Oxide Film." Journal of Nanomaterials 2015.1 (2015): 371405.